https://doi.org/10.5194/egusphere-2026-6918
Preprint. Discussion started: 23 November 2026
© Author(s) 2026. CC BY 4.0 License.

Tidal controls on soil and water CO_2 and CH_4 emissions in an Amazon estuarine floodplain forest

José Henrique Cattanio [a,c,*], Mario Flores Aroni [a,b]

[a] Graduate Program in Environmental Sciences, Federal University of Pará, Belém, Brazil

[b] Faculty of Agricultural Sciences, Professional School of Agricultural Engineering, National University of Altiplano, Puno, Peru

[c] Biogeochemical Cycles Laboratory, Federal University of Pará, Belém, Brazil

* Corresponding author: cattanio@ufpa.br (J.H. Cattanio).

Abstract

Amazon estuarine floodplain forests are periodically inundated by macrotides, creating dynamic redox conditions that regulate CO_2 and CH_4 emissions. However, few studies have simultaneously measured soil and water fluxes within the same tide-influenced system across seasons. We investigated how tidal phase (flood vs. ebb), compartment (water vs. soil), season (rainy vs. dry), and tide type (spring vs. neap) affect CO_2 and CH_4 emissions in a floodplain forest near Belém. Fluxes were measured hourly over complete tidal cycles using closed static chambers and automated GHG analyzers at the soil–atmosphere and water–atmosphere interfaces, across eight campaigns (four per season) covering spring and neap tides. Soil dominated CO_2 emissions, while water dominated CH_4 emissions. Ebb tide increased emissions relative to flood tide, especially for water CH_4 and CO_2. The compartment × tidal phase interaction was significant for CO_2 but not for CH_4; season and tide type had no effect. CO_2 and CH_4 are functionally decoupled between compartments, with tidal phase acting as a short-term driver. Integrated soil–water sampling across diurnal and tidal cycles is essential to quantify GHG balances in these ecosystems.

Keyword: Amazon estuary; tidal forest; floodplain; greenhouse gases.

1 INTRODUCTION

The rising atmospheric concentration of greenhouse gases (GHG), driven by anthropogenic activities, has intensified global warming (IPCC, 2001, 2014). Carbon dioxide (CO_2) is the primary anthropogenic GHG in terms of radiative forcing contribution, while methane (CH_4), although present at lower atmospheric

https://doi.org/10.5194/egusphere-2026-6918
Preprint. Discussion started: 23 November 2026
© Author(s) 2026. CC BY 4.0 License.

concentrations, exhibits a global warming potential 84 times greater than CO_2 over a 20-year horizon (IPCC, 2014; WMO, 2015). In this context, quantifying the sources and processes that control CO_2 and CH_4 emissions from terrestrial and aquatic ecosystems is essential for understanding the global carbon balance.

The islands of the Amazon estuary are formed by the deposition of Andean sediments (400-1000 × 10^6 t yr^{-1}) transported approximately 3,500 km to the river mouth, where they have accumulated since the Holocene on floodplains and the continental shelf (Nittrouer & Kuehl, 1995). This process is amplified by the region's macrotidal regime and high rainfall, which favor the deposition of silt-clay material and the formation of extensive, periodically inundated plains (Gregório & Mendes, 2009b, 2009a). These plains support the dense alluvial ombrophilous forest (estuarine floodplain forest), which covers approximately 40,000 km^2 downstream of the confluence of the Xingu and Amazon rivers (Anderson, 1990; Pires & Prance, 1985). This diverse and dynamic landscape harbors species of high commercial value (José H. Cattanio et al., 2002). Although its soils exhibit a high carbon storage capacity, decomposition processes under anaerobic conditions, associated with periodic flooding, result in significant CO_2 and CH_4 emissions (Aroni et al., 2026), making these ecosystems relevant contributors to global CH_4 emissions (Potter et al., 2014).

Soil CO_2 flux arises primarily from the combined production of autotrophic and heterotrophic respiration, with abiotic processes such as geochemical exchanges playing a minor role (Han & Zhu, 2020; Wang et al., 2020). The magnitude of these dynamics is regulated especially by soil moisture (Davidson et al., 2000), soil temperature (Bowden et al., 1998), and oxygen availability (Blagodatsky & Smith, 2012). In floodplain ecosystems, precipitation directly affects the respiratory activity of soil organisms and gas diffusion through the soil profile by modulating soil moisture (Bond-Lamberty et al., 2018; Davidson et al., 1998). In this environments, an additional key factor is the daily water level fluctuation driven by macrotides, as periodic inundation-drainage alter soil saturation and oxygenation, thereby regulating gas diffusion and redox conditions (Aroni et al., 2026; X. Liu et al., 2026).

Oxygen availability also determines the pathways of organic matter decomposition and CH_4 production. Methanogenesis, the final step of anaerobic organic matter degradation carried out by methanogenic archaea, is the primary pathway of CH_4 production (Conrad et al., 2011). However, the net emission of CH_4 to the atmosphere

https://doi.org/10.5194/egusphere-2026-6918
Preprint. Discussion started: 23 November 2026
© Author(s) 2026. CC BY 4.0 License.

depends on the balance between production, oxidation, and transport, which can occur via diffusion, ebullition, and plant-mediated transport (Conrad, 1996). Among the main natural sources of this gas are wetlands and inland waters (Kirschke et al., 2013). It is estimated that rivers, streams, and lakes collectively emit 26.8 Tg CH_4 yr^{-1} globally (Stanley et al., 2016), underscoring the importance of fluvial systems as CH_4 sources to the atmosphere.

Although soils and water share microbial processes for GHG production, their emission dynamics differ significantly. In soils, a substantial portion of carbon flux is associated with aerobic respiration by roots and microorganisms, however, water saturation reduces oxygen availability, altering the balance between aerobic and anaerobic processes (Conrad, 1996). In rivers and streams, organic carbon imported from adjacent terrestrial ecosystems is mineralized and emitted as CO_2 and CH_4 (Sawakuchi et al., 2017; Stanley et al., 2016). Under low-oxygen conditions, this organic matter input stimulates CH_4 production (Aroni et al., 2025; Barbosa et al., 2020).

Among these aquatic systems, tide-influenced Amazon rivers exhibit high concentrations of organic carbon derived from the nutrient-rich floodplains (Abril et al., 2014; Sawakuchi et al., 2017). This carbon is mineralized along the aquatic continuum, with CO_2 effluxes potentially increasing by up to 50% during high-water periods (Almeida et al., 2017). The semidiurnal tidal cycle controls hydrology and carbon exchange by alternating aerobic and anaerobic conditions, influencing both soil respiration and CH_4 production via methanogenesis in sediments and the water column (Wei et al., 2020). Although the importance of Amazonian wetlands for CH_4 emissions (Potter et al., 2014), no study has simultaneously measured CO_2 and CH_4 fluxes from both freshwater and soil under direct tidal influence. To address this gap, the present study simultaneously investigated CO_2 and CH_4 emissions in an Amazon floodplain forest connected to a tidal stream, which allowed us to evaluate the relative contribution of soil and water to GHG emissions within a single tide-influenced system.

2 MATERIAL AND METHODS

2.1 Study Area Location

Combú Island is an Environmental Protection Area covering approximately 15 km^2 that comprises a typical ecosystem of estuarine floodplain in the Brazilian Amazon

https://doi.org/10.5194/egusphere-2026-6918
Preprint. Discussion started: 23 November 2026
© Author(s) 2026. CC BY 4.0 License.

(Figure 1). Sampling was carried out in a tidal stream whose flow direction reverses with the tide, as water flows into the forest during flood tide and back toward the Combú channel during ebb tides, thereby promoting periodic soil inundation (Figure 1d). The geographic coordinates of the sampling point in the creek were 48°27'30.4056"W, 1°29'52.0512"S, while the soil sampling point was located at 48°27'23.5008"W, 1°29'58.3044"S (Figure 1d).

Figure 1 – Location of the study area: a) Brazil in South America; b) Belém municipality (blue outline); c) Combú Island Environmental Protection Area; and d) sampling locations in the water (blue circle) and soil (black circle).

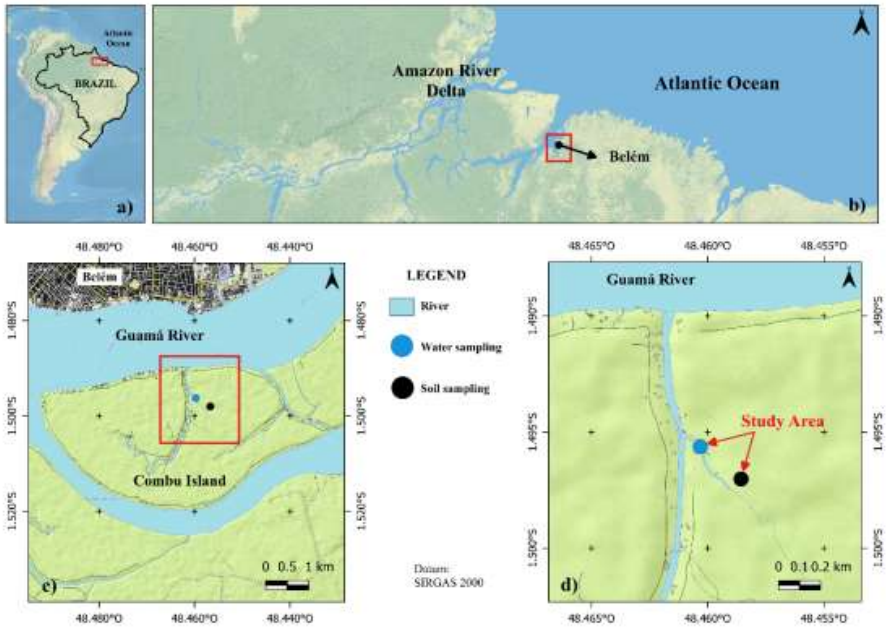

Source: altitude data (http://www.dsr.inpe.br/topodata/) with open access

The region has a mean annual air temperature of 27.0 °C and mean annual precipitation of 2,833 mm yr^{-1}, which can reach up to 4,505.1 mm yr^{-1} (Aroni et al., 2026). The climate is classified as Af according to the Köppen classification (Peel et al., 2007), with a rainy season concentrated between January and June and a less rainy season between July and December. Soils are classified as low-humic Gleysols (Silva & Sampaio, 1998).

https://doi.org/10.5194/egusphere-2026-6918
Preprint. Discussion started: 23 November 2026
© Author(s) 2026. CC BY 4.0 License.

2.2 Experimental Design

The months with the highest (March) and lowest (September) precipitation were selected for analysis, along with July and December to capture conditions at the transition between seasonal periods. Measurements were conducted on spring (highest amplitude) and neap (lowest amplitude) tides. For spring tides (Figure 2a) sampling began at low tide (start of flood), whereas for neap tides (Figure 2b) sampling started at high tide (beginning of ebb). This strategy allowed us to evaluate separately the effects of tidal amplitude and phase on GHG fluxes. Spring tide campaigns were conducted on 09/03/2020, 07/07/2020, 16/09/2020, and 01/12/2020, while neap tide campaigns occurred on 19/03/2020, 13/07/2020, 08/09/2020, and 09/12/2020. Measurements were performed at hourly intervals between 7:00 AM and 5:00 PM, starting 30 minutes before the predicted low or high tide based on Brazilian Navy Hydrographic Center tables. Soil and water surface fluxes were measured simultaneously to allow direct comparison between compartments.

Figure 2 – Schematic representation of tide types: (a) spring tide (flood) and (b) neap tide (ebb). The blue sphere indicates the start time of measurements.

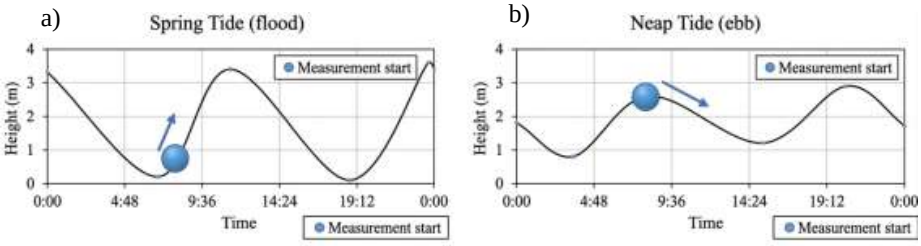

a) Spring Tide (flood) b) Neap Tide (ebb)

For soil CO_2 and CH_4 flux measurements, four PVC collars (12.0 cm height, 19.2 cm internal diameter) were installed at 2.0 cm into the soil and kept in the same location throughout the study, using the same site as used by Aroni et al. (2026). The collars were arranged in a circle 700 cm in diameter. For water-air interface measurements, a dynamic floating chamber (area of 804.0 cm^2 and volume of 9,650 cm^3) was used, following design described by Castellón et al. (2021). Fluxes form both compartments (stream and soil) were measures throughout the tidal cycle rather than independent temporal replicates (Huang et al., 2019; Norman et al., 1997). The four PVC collars were considered spatial replicates of the same sampling point, and their measurements were pooled by collection day to compose the experimental unit (campaign). Thus, the experimental unit considered in the statistical analyses was the

https://doi.org/10.5194/egusphere-2026-6918
Preprint. Discussion started: 23 November 2026
© Author(s) 2026. CC BY 4.0 License.

sampling day (n = 8), with hourly measurements and collars treated as repeated measures nested in time and space.

2.3 Environmental Characterization

Physicochemical properties of the water column were measured at depths of up to 90.0 cm using a HORIBA multiparameter probe (Model U51-G). The following variables were recorded: water temperature (Tw; °C), hydrogen potential (pH), oxidation-reduction potential (ORP; mV), electrical conductivity (EC; µS cm^{-1}), turbidity (Turb.; NTU), dissolved oxygen (DO; %), and total dissolved solids (TDS; g L^{-1}). Soil surface temperature (Ts; °C) was measured at a depth of up 3.0 cm using a portable digital thermometer (model TP101). At 100 cm above the ground, we measured air temperature (Ta; °C), relative humidity (RH; %), wind speed (WS; m s^{-1}) and atmospheric pressure (P; hPa) using a multifunctional digital anemometer. All variables were recorded concurrently with GHG flux measurements.

Precipitation data were obtained from the Brazilian National Institute of Meteorology (INMET, 2025) using the meteorological station located in Belém (01°26’09,00”S; 048°26’14,00”W), approximately 6.5 km from the study site. Tide data were provided by the Brazilian Navy Hydrographic Center (Marinha do Brasil, 2020) based on the Belém port station (01°26'2.5"S; 048°29'36"W).

2.4 The CO_2 and CH_4 Flux Measurements in Water and Soil

The CO_2 and CH_4 fluxes at the soil-atmosphere and water-atmosphere interfaces were measured using the closed static chamber method with two automated ultra-portable GHG analyzers (Model 915–0011, Los Gatos Research, USA) in a closed-loop configuration (Mahesh et al., 2015). Analyzers were calibrated monthly with high-purity standards (500 ppm CO_2, 5 ppm CH_4) and recorded concentrations at 2-second intervals. For soil measurements, PVC collars were sequentially sealed with lids for 3.0 min, followed by 1.0 min of re-equilibration with the atmosphere, and this cycle was repeated for each of the four chambers (Aroni et al., 2026). For water measurements, the floating chamber was positioned over the water surface for the same 3.0-min period, with the same re-equilibration procedure repeated for four cycles (Castellón et al., 2021; Jacotot et al., 2018). Internal volumes of the soil collars were measured at the end of each sampling day using a millimeter ruler (four heights per collar), with total volume

https://doi.org/10.5194/egusphere-2026-6918
Preprint. Discussion started: 23 November 2026
© Author(s) 2026. CC BY 4.0 License.

calculated as collar plus lid volume. The floating chamber has a fixed, pre-determined internal volume, requiring no field measurements.

2.5 CO_2 and CH_4 Flux Calculation

The CO_2 and CH_4 fluxes between the surfaces (soil and water) and the atmosphere were determined from the rate of change in gas concentration (ppm) inside the chamber over time, according to the following equation:

$$F = (P \times V \times M \times U \times (dc/dt)) / (A \times T \times R)$$

Where F is the gas flux (g CO_2 m^{-2} d^{-1} or g CH_4 m^{-2} d^{-1}); P is the atmospheric pressure (atm); V is the effective internal volume of the chamber (L); M is the molecular mass of CO_2 (44 g mol^{-1}) or CH_4 (16 g mol^{-1}); U is the conversion factor (86400 s d^{-1}); A is the surface area covered by the chamber (m^2); R is the universal gas constant (0.08205 L atm K^{-1} mol^{-1}); T is the temperature (K); and dc/dt is the slope of the linear regression fitted between gas concentration (ppm) and time (s). Fluxes were calculated from the rate of increase/decrease in concentration over time after chamber closure, adjusted for chamber volume and coverage area (Abichou et al., 2006; Davidson et al., 2000; Nakano et al., 2004). Only regressions with $R^2 > 0.85$ were retained for flux calculations (Huttunen et al., 2002).

2.6 Statistical Analysis

All statistical analyses were performed using R version 4.6 (Team, 2018) with the following packages: lme4 (Bates et al., 2015), lmerTest (Kuznetsova et al., 2017), emmeans (Lenth & Piaskowski, 2017), car (Fox & Weisberg, 2019), Hmisc (Harrell Jr, 2003), dplyr (Wickham et al., 2026), tidyr (Wickham et al., 2014), readxl (Wickham & Bryan, 2015) and ggplot2 (Wickham, 2016). Additionally, the corrplot package was used for visualizing correlation matrices. Data were organized in long format, with response variables (gas fluxes and physicochemical parameters of water and soil) and fixed factors (compartment, tidal phase, seasonality, and tidal type). Initially, descriptive statistics were computed. Normality and homogeneity of variances were assessed on model residuals (not on raw data) using Shapiro–Wilk and Levene's tests, respectively, after model fitting.

To evaluate the effects of compartment (water vs. soil) and tidal phase (flood vs. ebb) on CO_2 and CH_4 fluxes, we fitted independent linear mixed-effects models (LMMs) for each gas, with the following structure: Gas_flux ~ Compartment *

https://doi.org/10.5194/egusphere-2026-6918
Preprint. Discussion started: 23 November 2026
© Author(s) 2026. CC BY 4.0 License.

Tidal_phase + (1 | Day/Replicate). Reduced models were fitted and explicitly reported whenever the full model did not converge or when higher-order interactions were not estimable due to an unbalanced design. Random effects included intercepts for Day (sampling days) and Replicate (measurement replicates within each day) to account for the hierarchical and temporal structure of the data. Fixed effects were tested using Type III Wald F tests with Satterthwaite's method for denominator degrees of freedom approximation, as implemented in the lmerTest package. Type III Wald F tests were used for fixed effects, and likelihood ratio tests (LRT, χ^2) were used for random effects and for comparing nested models. The interaction between compartment and tidal phase was assessed via Type III Wald F tests (car package), and simple-effects analyses were performed by slicing the interaction using the emmeans package when the interaction was significant. Post-hoc comparisons between factor levels were performed using the emmeans package with pairwise contrasts and Satterthwaite's degrees of freedom (lmer.df = "satterthwaite") and Tukey's adjustment for multiple comparisons when applicable. Contrasts between tidal phases within each compartment were obtained using contrast (method = "trt.vs.ctrl", ref = "Flood"). Ratios between model-estimated means were computed on the log scale, and 95% confidence intervals (CIs) were obtained from the model using the Delta method (or parametric bootstrap with 10,000 resamples when the Delta method was not applicable). Ratios were considered statistically significant when the 95% CI did not include 1. The effects of season (wet vs. dry) and tidal type (spring vs. neap) on fluxes were evaluated separately in complementary models: Gas flux ~ Season + (1 | Day/Replicate) and Gas flux ~ Tidal_type + (1 | Day/Replicate), respectively. When the compartment × tidal phase interaction was significant, main effects were not interpreted in isolation, instead, simple effects were analyzed within each level of the interacting factor.

For water physicochemical characteristics (temperature, pH, EC, DO, Turb., ORP, and TDS), independent linear mixed-effects models were fitted for each parameter following the structure: Parameter ~ Tidal_phase + Season + Tidal_type + (1 | Day) + (1 | Replicate). When the three-way interaction was not significant, it was removed and the model was refitted. For soil environmental parameters (Ts, Ta, RH, WS, and P), analogous models were applied. Differences between tidal phases within each season × tidal type combination for environmental parameters (Tables 1 and 2) were assessed using the Kruskal-Wallis test, with significance level at $\alpha = 0.05$.

https://doi.org/10.5194/egusphere-2026-6918
Preprint. Discussion started: 23 November 2026
© Author(s) 2026. CC BY 4.0 License.

The relationships between CH_4 and CO_2 fluxes and physicochemical parameters were assessed using Spearman's rank correlation coefficient (ρ), with correlation matrices constructed separately by compartment (water and soil) and tidal phase (flood and ebb). To account for temporal pseudoreplication, the number of effective observations was based on the number of independent sampling days when appropriate. To control for false discovery rate due to multiple comparisons, p-values from Spearman correlations were adjusted using the Benjamini–Hochberg procedure (FDR) at $\alpha = 0.05$. Model assumptions (normality and homoscedasticity of residuals) were verified visually through residual plots and confirmed with Shapiro–Wilk tests applied to model residuals. When assumptions were violated, data were log-transformed using log(x+1) to accommodate zero and negative values in CH_4 fluxes and models were refitted. All tests were two-tailed, and the significance level was set at $\alpha = 0.05$. Results are presented as means ± standard error (SE) or as coefficient estimates with 95% confidence intervals (CI). In cases where the LMM with the full random-effects structure (1|Day/Replicate) was singular, a reduced model with (1|Day) was fitted and reported, and this simplification is indicated in the text.

3 RESULTS

3.1 General Patterns

3.1.1 CO_2 Fluxes

Soil acted as the primary source of CO_2 to the atmosphere (Figure 3A), with fluxes significantly higher than those from water during both tidal phases. During flood tide, soil fluxes (10.599 ± 0.889 g CO_2 m^{-2} d^{-1}, n = 116) exceeded water fluxes (3.531 ± 0.287 g CO_2 m^{-2} d^{-1}), with a mean paired difference of 7.229 ± 0.954 g CO_2 m^{-2} d^{-1} (Figure 3B). During ebb tide, soil fluxes (14.273 ± 0.736 g CO_2 m^{-2} d^{-1}, n = 196) also exceeded water fluxes (8.202 ± 1.136 g CO_2 m^{-2} d^{-1}, n = 196), with mean paired difference of 6.128 ± 1.500 g CO_2 m^{-2} d^{-1} (paired t-test: $t = 4.070$, $df = 191$, $p < 0.001$) (Figure 3B). The linear model (Figure 3C) indicated a significant effect of tidal phase ($F = 12.390$; $df = 625.180$; $p < 0.001$) and season ($F = 7.530$; $p = 0.006$), as well as significant interactions between compartment and season ($F = 5.824$; $p = 0.016$) and between tidal phase and season ($F = 4.325$; $p = 0.038$). The main effect of compartment ($F = 19.041$; $df = 629.580$; $p < 0.001$) was significant (Figure 3D).

https://doi.org/10.5194/egusphere-2026-6918
Preprint. Discussion started: 23 November 2026
© Author(s) 2026. CC BY 4.0 License.

Figure 3 – CO_2 fluxes (FCO2) in water and soil compartments. (A) Boxplot of CO_2 fluxes by compartment; (B) Mean CO_2 emission intensity; (C) Fixed effects of the linear model for CO_2; (D) Difference between CO_2 fluxes during ebb and flood tides by compartment. Error bars represent standard errors; different letters indicate significant differences ($p < 0.05$).

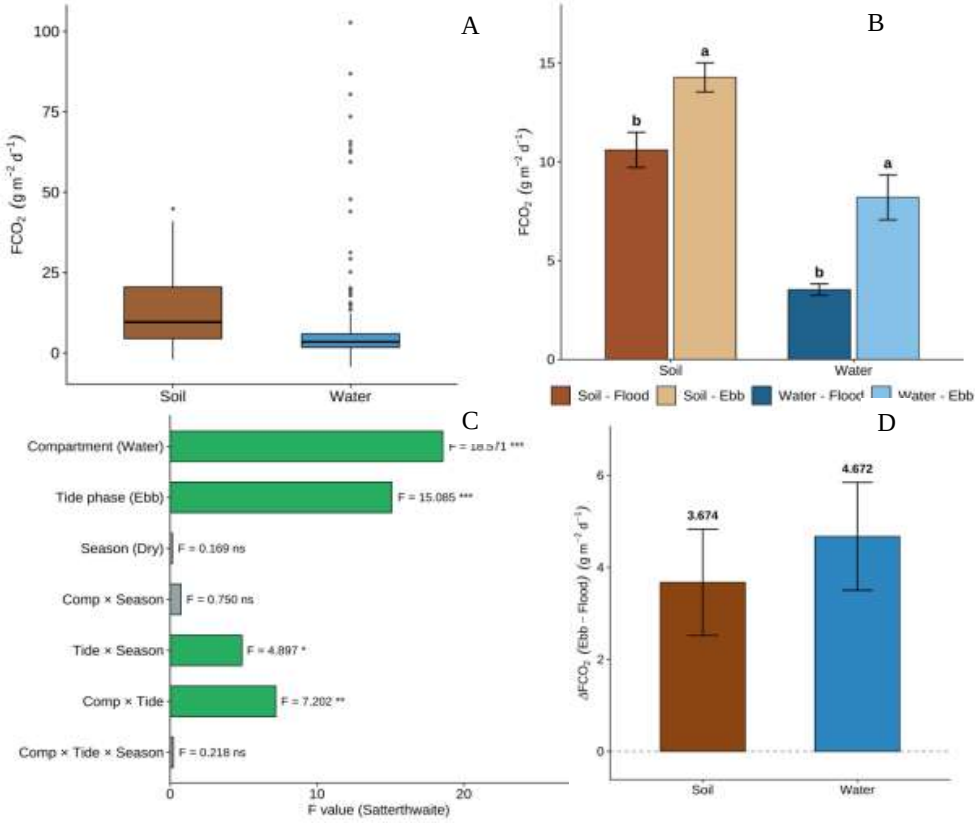

CH_4 Fluxes

In contrast to CO_2, water exhibited higher mean CH_4 fluxes than soil, with an overall mean difference of 0.450 ± 0.087 g CH_4 m^{-2} d^{-1} (Figure 4A). A non-significant interaction between compartment and tidal phase was observed (F = 0.636; df = 605.510; p = 0.426; Figure 4D). During flood tide (Figure 4B), no significant difference was observed between CH_4 fluxes from water (0.173 ± 0.067 g CH_4 m^{-2} d^{-1}) and soil (0.015 ± 0.004 g CH_4 m^{-2} d^{-1}; p = 0.299). However, during ebb tide, water (0.665 ± 0.137 g CH_4 m^{-2} d^{-1}) emitted significantly more CH_4 than soil (0.019 ± 0.003 g CH_4 m^{-2} d^{-1}; $p < 0.001$), with a difference of 0.646 ± 0.137 g CH_4 m^{-2} d^{-1} (Figure 4B). Thus, the overall significance of the water-soil difference was largely driven by ebb-tide

https://doi.org/10.5194/egusphere-2026-6918
Preprint. Discussion started: 23 November 2026
© Author(s) 2026. CC BY 4.0 License.

conditions, highlighting the modulating role of tidal phase on CH_4 emissions. Negative CH_4 fluxes accounted for 23.9% of all observations (Figure 4C).

Figure 4 – CH_4 fluxes (FCH4) in water and soil compartments. (A) Boxplot of CH_4 fluxes by compartment; (B) Comparison of CH_4 fluxes between water and soil during flood and ebb tides; (C) Proportion of CH_4 sources, sinks, and neutral fluxes; (D) Interaction between compartment and tidal phase for CH_4 fluxes (fixed effects of the linear model). Error bars represent standard errors; different letters indicate significant differences ($p < 0.05$).

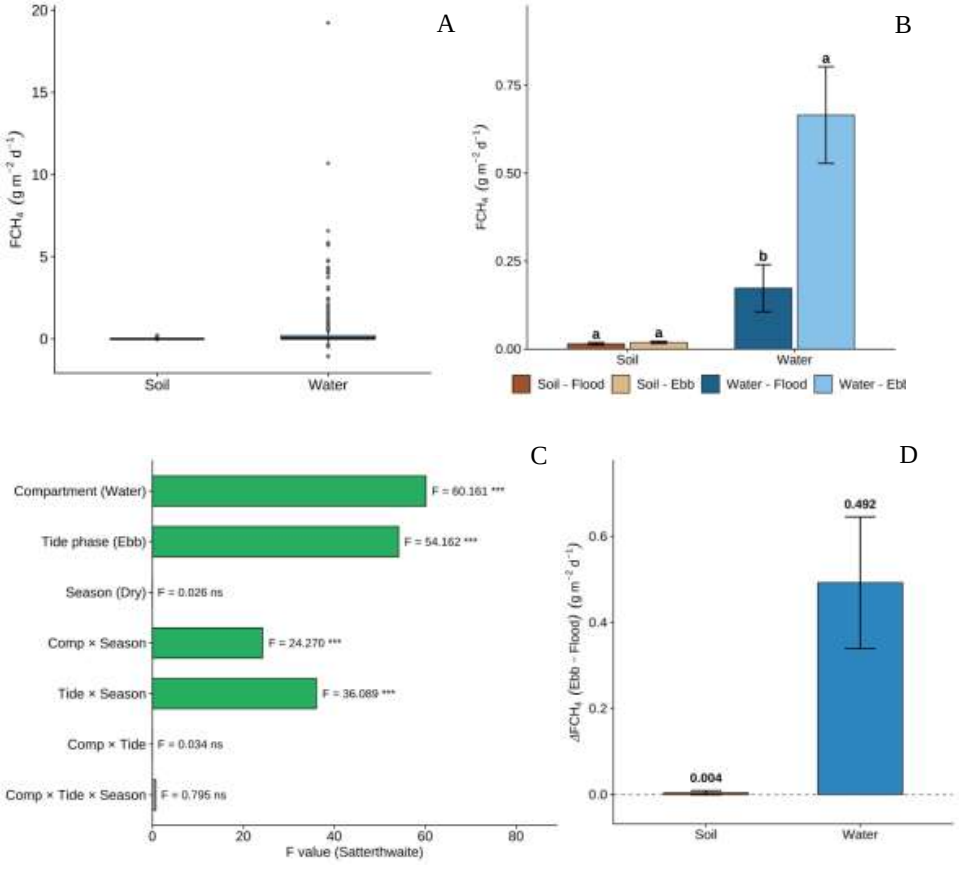

3.2 Tidal Effects on Gas Fluxes

Tidal phase exerted a modulating role on gas fluxes, with more pronounced effects on the water compartment. For CO_2, ebb tide increased emissions by 1.350-fold (95% CI: 1.113–1.646; $p < 0.01$) and water emissions by 2.320-fold (95% CI: 1.668–3.162; $p < 0.001$); the compartment × tidal phase interaction was significant ($F = 7.470$;

https://doi.org/10.5194/egusphere-2026-6918
Preprint. Discussion started: 23 November 2026
© Author(s) 2026. CC BY 4.0 License.

df = 629.790; $p < 0.01$). For CH_4, ebb tide did not significantly increase soil emissions (1.260-fold; 95% CI: 0.714-2.466; $p = 0.432$), whereas water emissions increased 3.850-fold (95% CI: 1.785-11.154; $p = 0.001$) (Figure 4C). The compartment × tidal phase interaction was not significant for CH4 ($F = 0.636$; df = 605.510; $p = 0.426$; Figure 4D).

3.3 Seasonal and Tidal-Type Effects

Seasonality exerted distinct effects on CO_2 and CH_4 fluxes, with opposite responses between the aquatic and terrestrial compartments for CO_2 (Figure 5), although no significant differences were detected for CH_4. Tidal type (spring vs. neap) also did not significantly influence CO_2 emissions ($p > 0.05$). In the water column, CO_2 fluxes were numerically higher during the wet season (9.646 ± 1.404 g CO_2 m^{-2} d^{-1}) compared to the dry season (3.308 ± 0.229g CO_2 m^{-2} d^{-1}), with a wet/dry ratio of 2.920 (95% CI: 2.080-3.960), but this difference was not significant ($F = 0.070$; df = 5.975; $p = 0.800$). In soil, fluxes were numerically higher in the dry season (13.742 ± 0.844 g CO_2 m^{-2} d^{-1}) than in the wet season (11.881 ± 0.753 g CO_2 m^{-2} d^{-1}), with a wet/dry ratio of 0.865 (95% CI: 0.725-1.030), also without significant difference ($F = 0.756$; df = 30.107; $p = 0.391$).

Figure 5 – CO_2 fluxes (FCO2) from water (blue) and soil (brown) during A) spring tide in the rainy season, during flood and ebb; B) spring tide in the dry season, during flood and ebb phases; C) neap tide in the rainy season, during flood and ebb; D) neap tide in the dry season, during flood and ebb.

https://doi.org/10.5194/egusphere-2026-6918
Preprint. Discussion started: 23 November 2026
© Author(s) 2026. CC BY 4.0 License.

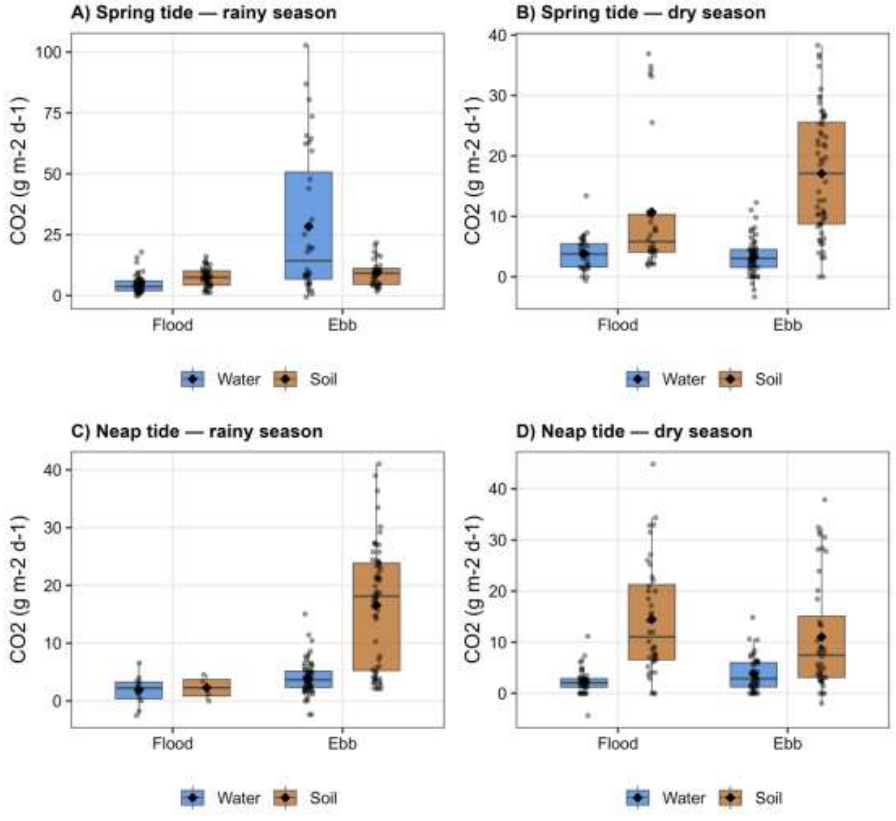

For FCH4 (Figure 6), no significant seasonal effect was observed in water (wet: 0.411 ± 0.150 vs. dry: 0.518 ± 0.096 g CH_4 m^{-2} d^{-1}; ratio = 0.792; 95% CI: 0.304–1.620; F = 1.339; df = 5.980; p = 0.291). In soil, fluxes were very low in both seasons (wet: 0.011 ± 0.003 vs. dry: 0.022 ± 0.004 g CH_4 m^{-2} d^{-1}), with a wet/dry ratio of 0.501 (95% CI: 0.272–0.879; F = 0.126; df = 5.996; p = 0.735). Ratios were calculated as the ratio between observed means. The 95% confidence intervals were obtained via bootstrap (10,000 resamples) and should not be interpreted as hypothesis tests for the ratio.

Figure 6 – CH_4 fluxes (FCH4) from water (blue) and soil (brown) during A) spring tide in the rainy season, during flood and ebb; B) spring tide in the dry season, during flood and ebb phases; C) neap tide in the rainy season, during flood and ebb; D) neap tide in the dry season, during flood and ebb.

https://doi.org/10.5194/egusphere-2026-6918
Preprint. Discussion started: 23 November 2026
© Author(s) 2026. CC BY 4.0 License.

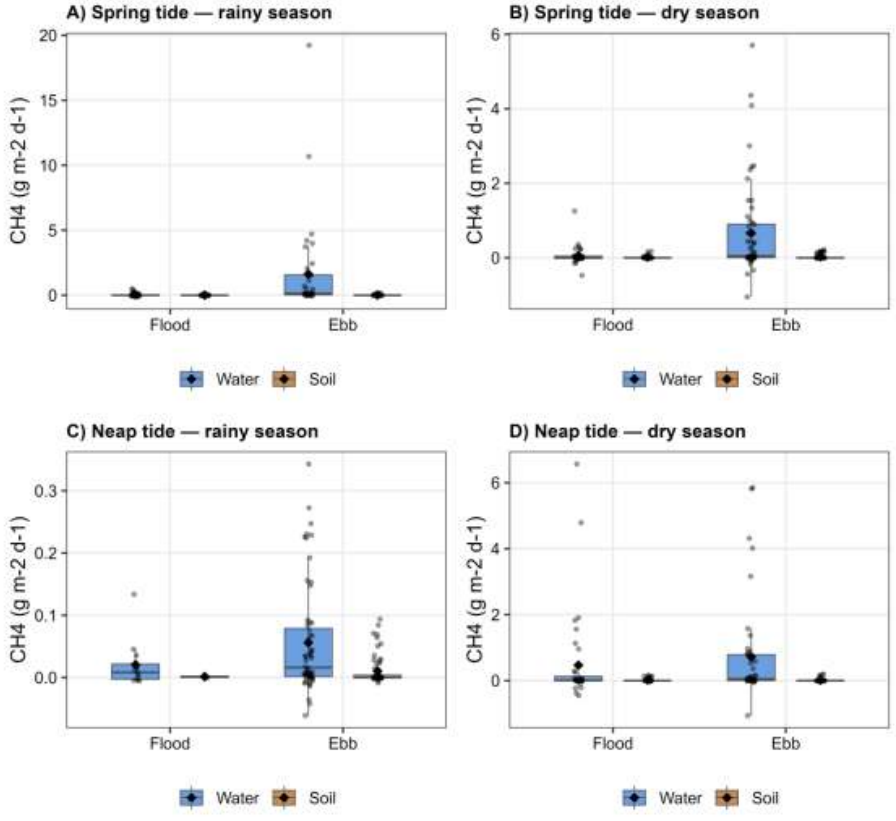

3.4 Paired Comparisons Under Specific Conditions

Direct comparisons between the two compartments under each specific condition revealed patterns consistent with the overall results. For CO_2, soil emissions were significantly higher than water emissions across all combinations ($p < 0.001$), with soil-to-water ratios of 3.00 (flood tide) and 1.74 (ebb tide), calculated from model-estimated means (Figure 3B). For CH_4, although the global analysis across all combinations indicated that water emissions significantly exceeded soil emissions ($p < 0.001$), this difference was not significant in the flood-tide comparison ($p = 0.299$; Figure 4B). The highest CH_4 flux was observed in water during the spring ebb tide in the rainy season (1.620 ± 0.615 g m^{-2} d^{-1}; Figure 6), a value approximately 40-fold higher than the soil flux under the same conditions (0.047 ± 0.009 g m^{-2} d^{-1}; see Table S1 for detailed results).

https://doi.org/10.5194/egusphere-2026-6918
Preprint. Discussion started: 23 November 2026
© Author(s) 2026. CC BY 4.0 License.

Correlation analyses showed no significant relationship between water and soil CO_2 fluxes (ρ = -0.045; p = 0.426; n = 308). Tidal height was negatively correlated with water CO_2 fluxes (ρ = -0.397; p < 0.001), whereas water FCO2 and FCH4 were positively correlated with each other (ρ = 0.354; p < 0.001). The FCH4 in water and soil were weakly negatively correlated (ρ = -0.134; p = 0.019), while CO_2 and CH_4 in soil were not significantly correlated (ρ = 0.088; p = 0.122).

3.5 Physicochemical Parameters

Variations in water physicochemical parameters showed that, overall, Tw and pH differed significantly between tidal phases, with patterns varying according to tidal type and seasonal period (Table 1). Oxidation-reduction potential (ORP), EC, and TDS were generally higher during either ebb or flood tides, depending on the specific conditions (Table 1). Turbidity and DO, in contrast, exhibited significant differences less frequently, and only in a few tide–season combinations (Table 1).

Table 1. Variation of water physicochemical parameters as a function of tidal type (spring and neap) and tidal phase (flood and ebb) during the rainy and dry seasons at Combú Island. Lowercase letters compare flood and ebb within each season (Kruskal–Wallis test, p < 0.05); (–) indicates no significant variation. Water temperature (Tw; °C); Oxidation–reduction potential (ORP; mV); EC: electrical Eletrical conductivity (EC; µS cm^{-1}); Turbidity (Turb.; NTU); Dissolved oxygen (DO; %); Total dissolved solids (TDS; g L^{-1}).

Tidal type	Season	Tidal phase	Tw	pH	ORP	EC	Turb.	DO	TDS
Spring	Rainy	Flood	28.86 ± 0.34^{b}	5.46 ± 0.07^{a}	422.83 ± 6.54^{-}	47.25 ± 2,60^{-}	38.74 ± 1.34^{a}	56.63 ± 2.20^{-}	0.031 ± 0.002^{-}
		Ebb	30.05 ± 0.21^{a}	5.21 ± 0.03^{b}	438.00 ± 4.89^{-}	44.35 ± 2.33^{-}	31.96 ± 0.93^{b}	54.57 ± 2.98^{-}	0.029 ± 0.001^{-}
	Dry	Flood	30.01 ± 0.18^{-}	6.17 ± 0.07^{a}	355.84 ± 5.43^{b}	50.78 ± 5.43^{a}	21.39 ± 3.04^{a}	62.88 ± 5.70^{-}	0.033 ± 0.002^{a}
		Ebb	30.35 ± 0.13^{-}	5.75 ± 0.09^{b}	386.38 ± 9.69^{a}	38.79 ± 2.04^{b}	11.74 ± 1.80^{b}	63.13 ± 2.84^{-}	0.025 ± 0.001^{b}
Neap	Rainy	Flood	29.90 ± 0.32^{-}	6.19 ± 0.04^{a}	356.83 ± 9.79^{-}	68.17 ± 2,30^{a}	25.99 ± 2.51^{-}	29.72 ± 3.47^{b}	0.044 ± 0.001^{a}
		Ebb	29.31 ± 0.09^{-}	5.93 ± 0.06^{b}	391.58 ± 7.54^{-}	38.88 ± 1.83^{b}	20.89 ± 0.67^{-}	48.81 ± 2.53^{a}	0.026 ± 0.001^{b}

https://doi.org/10.5194/egusphere-2026-6918
Preprint. Discussion started: 23 November 2026
© Author(s) 2026. CC BY 4.0 License.

	Dry	Flood	29.59 ± 0.17[b]	6.24 ± 0.15[-]	345.55 ± 9.15[b]	50.23 ± 3.15[a]	13.96 ± 1.15[-]	56.97 ± 4.25[-]	0.033 ± 0.002[a]
		Ebb	30.65 ± 0.06[a]	5.91 ± 0.13[-]	390.93 ± 7.83[a]	36.00 ± 2,31[b]	14.84 ± 0.74[-]	64.18 ± 3.92[-]	0.024 ± 0.002[b]

3.6 Environmental Correlations

Soil temperature and Ta were numerically higher during ebb tides in several conditions, although significant differences were restricted to specific season–tidal type combinations (Table 2). Soil temperature (Ts) was significantly higher at ebb during the rainy season under spring tides and during the dry season under neap tides. Air temperature (Ta) was higher at ebb only during spring tides in the rainy season. Relative humidity (RH) was higher at flood under specific conditions (neap tides, dry season), whereas P was higher at flood only during spring tides in the rainy season. Tidal height (TH) and WS showed no significant variation between tidal phases (Table 2).

Table 2. Variation of environmental parameters in the floodplain forest as a function of tidal type (spring and neap) and tidal phase (flood and ebb) during the rainy and dry seasons. Lowercase letters indicate significant differences between flood and ebb within the same season (Kruskal–Wallis test, $p < 0.05$); (-) denotes no significant variation. Soil temperature (Ts; °C); Air temperature (Ta; °C); Relative humidity (%); wind speed (WS; m s^{-1}); P: atmospheric pressure (hPa); TH: mean tidal height (m).

Tidal type	Season	Tidal phase	Ts	Ta	RH	WS	P	TH
Spring	Rainy	Flood	26.92 ± 0.28[b]	28.56 ± 0.56[-]	85.62 ± 2.05[-]	0.00 ± 0.00[-]	1013.17 ± 0.24[a]	2.04 ± 0.28[-]
		Ebb	28.16 ± 0.15[a]	30.44 ± 0.17[-]	83.98 ± 1.31[-]	0.00 ± 0.00[-]	1010.02 ± 0.34[b]	1.96 ± 0.20[-]
	Dry	Flood	27.28 ± 0.44[-]	31.15 ± 1.26[-]	72.30 ± 4.24[-]	0.00 ± 0.00[-]	1009.94 ± 0.52[-]	1.93 ± 0.28[-]
		Ebb	27.88 ± 0.27[-]	31.19 ± 0.82[-]	72.57 ± 2.56[-]	0.00 ± 0.00[-]	1010.41 ± 0.87[-]	1.87 ± 0.19[-]
Neap	Rainy	Flood	27.35 ± 0.15[-]	28.50 ± 0.04[-]	86.20 ± 2.79[-]	0.00 ± 0.00[-]	1008.40 ± 0.51[-]	1.61 ± 0.15[-]
		Ebb	27.61 ± 0.17[-]	30.11 ± 0.68[-]	79.17 ± 2.47[-]	0.06 ± 0.06[-]	1007.95 ± 2.49[-]	1.84 ± 0.16[-]

https://doi.org/10.5194/egusphere-2026-6918
Preprint. Discussion started: 23 November 2026
© Author(s) 2026. CC BY 4.0 License.

	Dry	Flood	27.67 ± 0.28[b]	29.81 ± 1.17[-]	82.33 ± 3.20[a]	0.00 ± 0.00[-]	1012.18 ± 0.59[-]	1.83 ± 0.28[-]
		Ebb	28.87 ± 0.20[a]	31.29 ± 0.80[-]	71.97 ± 2.88[b]	0.13 ± 0.13[-]	1011.63 ± 0.44[-]	1.79 ± 0.23[-]

3.7 Correlations Between Gas Fluxes and Environmental Parameters

Spearman correlation analysis (Table 3) revealed associations between gas fluxes and various environmental parameters, with a greater number and magnitude of correlations observed during ebb tides.

3.7.1 Correlations in the Water Compartment

For water FCO_2 (Table 3), when considering tidal phases separately, tidal height showed the highest correlation magnitudes in both phases, with a stronger correlation during ebb tides ($\rho = -0.601$; $p < 0.001$) than during flood tides ($\rho = -0.341$; $p > 0.05$). During flood tides, Tw ($\rho = -0.380$; $p > 0.05$), EC ($\rho = 0.252$; $p > 0.05$), and ORP ($\rho = -0.300$; $p > 0.05$) were not significantly correlated with FCO2. During ebb tides, the strongest correlations were observed with tidal height ($\rho = -0.601$; $p < 0.001$), EC ($\rho = 0.476$; $p < 0.001$), TDS ($\rho = 0.460$; $p < 0.01$), DO ($\rho = -0.455$; $p < 0.01$), Tw ($\rho = -0.437$; $p < 0.001$), and pH ($\rho = -0.299$; $p < 0.05$). For water FCH4, tidal height was significantly correlated only during ebb tides ($\rho = -0.514$; $p < 0.001$), whereas no significant correlation was observed during flood tides ($\rho = -0.129$; $p > 0.05$). During ebb tides, EC ($\rho = 0.431$; $p < 0.01$) and TDS ($\rho = 0.434$; $p < 0.001$) were also significantly correlated with FCH4 . During flood tides, no significant correlation was observed between FCH4 and ORP ($\rho = 0.086$; $p > 0.05$).

Table 3. Spearman correlation coefficients (ρ) between gas fluxes (FCO2 and FCH4) and environmental parameters in the water and soil compartments: Tidal height (TH, m); Water temperature (Tw; °C); Hydrogen potential (pH); Dissolved oxygen (OD; %); Total dissolved solids (TDS; g L^{-1}); Electrical conductivity (EC.; µS cm^{-1}); Oxidation–reduction potential (ORP; mV); Turbidity (Turb.; NTU); Soil temperature (Ts; °C); Air temperature (Ta; °C); Relative humidity (RH; %); Wind speed (WS; m s^{-1}); Atmospheric pressure (P; hPa).

Parameters	Water	
	FCO2	FCH4

https://doi.org/10.5194/egusphere-2026-6918
Preprint. Discussion started: 23 November 2026
© Author(s) 2026. CC BY 4.0 License.

	Flood	Ebb	Total	Flood	Ebb	Total
TH	-0.341^{-}	-0,601***	-0.489***	-0.129^{-}	-0,514**	-0,360**
Tw	-0.380^{-}	-0.437**	-0,392**	-0.086^{-}	-0.242^{-}	-0.137^{-}
pH	0.191^{-}	-0.299	-0.123^{-}	0.222^{-}	0.094^{-}	0.105^{-}
OD (%)	-0.137^{-}	-0.455**	-0,329***	0.387^{-}	0.011^{-}	0.156^{-}
TDS	0,256^{-}	0.460**	0,350**	-0.182^{-}	0.434**	0.096^{-}
EC	0.252^{-}	0.476**	0,355**	-0.191^{-}	0.431**	0,095^{-}
ORP	-0.300^{-}	-0.193^{-}	-0.223^{-}	0.086^{-}	-0.174^{-}	-0.040^{-}
Turb.	-0.286^{-}	-0.077^{-}	-0.151^{-}	0.141^{-}	0.029^{-}	0.022^{-}
Parameters	Soil					
	FCO2			FCH4		
	Flood	Ebb	Total	Flood	Ebb	Total
Ts	0.312^{-}	0.074^{-}	0.169^{-}	-0.141^{-}	-0.153^{-}	-0.207^{-}
Ta	0.477^{-}	0.165^{-}	0.232^{-}	-0.211^{-}	-0.300^{-}	-0.310^{-}
RU	-0.345^{-}	-0.474*	-0.425**	0.003^{-}	0.336^{-}	0.331^{-}
WS		-0.241^{-}	-0.204^{-}		0.298^{-}	0.239^{-}
P	-0.323^{-}	0,157^{-}	-0.008^{-}	0.096^{-}	-0,086^{-}	0.066^{-}

*** < 0.001 (FDR adjusted); ** < 0.01 (FDR adjusted); * < 0.05 (FDR adjusted); (-) Not significant

3.7.2 Correlations in the Soil Compartment

In the soil compartment, FCO2 showed no significant correlations with Ts (ρ = 0.169; $p > 0.05$) or atmospheric pressure (ρ = -0.008; $p > 0.05$) across all observations. During flood tides, neither Ts (ρ = 0.312; $p > 0.05$) nor P (ρ = -0.323; $p > 0.05$) were significantly correlated with FCO2, nor was Ts during ebb tides (ρ = 0.074; $p > 0.05$). Only RH was significantly correlated with soil FCO2, showing a negative association during ebb tides (ρ = -0.474; $p < 0.001$) and across all observations (ρ = -0.425; $p < 0.001$). For soil FCH4, no significant correlations were observed with any of the evaluated environmental parameters (Table 3). This result indicates that no significant monotonic association was detected between soil FCH4 and the measured environmental variables under the conditions and temporal scale assessed.

https://doi.org/10.5194/egusphere-2026-6918
Preprint. Discussion started: 23 November 2026
© Author(s) 2026. CC BY 4.0 License.

4 DISCUSSION

A critical aspect of understanding the role of rivers in greenhouse gas fluxes to the ocean lies in quantifying the extent to which tidal dynamics influence the biogeochemical processes operating along river channels and floodplain areas. The results obtained in this study demonstrate that CO_2 and CH_4 fluxes differ markedly between soil and water compartments, and that tidal dynamics exert a significant influence on these fluxes, particularly on CH_4 emissions from the water column. This pattern aligns with recent findings from tropical and subtropical ecosystems (Aroni et al., 2026; Su et al., 2024; Tu et al., 2025).

4.1 Contrasting Emission Patterns of CO_2 and CH_4

Soil acted as the primary source of CO_2 to the atmosphere, with mean fluxes of 10.599 ± 0.889 g CO_2 m^{-2} d^{-1} during flood tide and 14.273 ± 0.736 g CO_2 m^{-2} d^{-1} during ebb tide, whereas water exhibited fluxes of 3.531 ± 0.287 g CO_2 m^{-2} d^{-1} and 8.202 ± 1.136 g CO_2 m^{-2} d^{-1}, respectively. Depending on the tidal phase, water accounted for 33–57% of soil fluxes on a per-area basis, underscoring the biogeochemical compartmentalization within estuarine floodplain areas. It is important to note that these comparisons refer to area-specific emission rates rather than the total ecosystem contribution of each compartment, which also depends on their respective spatial extents. These soil fluxes corroborate previous measurements from the same study area on high-elevation topography (16.084 ± 0.612 g m^{-2} d^{-1}), where values were found to be higher than those from low-elevation sites (Aroni et al., 2026). Furthermore, the acidic nature of floodplain waters (Table 1) is consistent with expectations of CO_2 emission, as organic matter decomposition in waterlogged soils releases organic acids that acidify the water column (Junk et al., 2011). Only aquatic CO_2 emissions (6.322 ± 0.700 g m^{-2} d^{-1}) exhibited significant diurnal variation ($F = 3.56$, $p < 0.001$), with values 165% higher after 12:00 h (local time). This diurnal pattern, often overlooked in short-term sampling campaigns, underscores the importance of sampling protocols that capture the full diel cycle for accurate emission estimates (Bass et al., 2013).

Spearman correlations between aquatic FCO2 and physicochemical variables, although weak to moderate, are consistent with the combined influence of physical and biogeochemical processes on CO_2 fluxes. The negative correlation between FCO2 and Tw during ebb tide ($\rho = -0.437$; $p < 0.001$) supports the hypothesis that enhanced photosynthesis, favored by higher temperature and light availability, may reduce

https://doi.org/10.5194/egusphere-2026-6918
Preprint. Discussion started: 23 November 2026
© Author(s) 2026. CC BY 4.0 License.

dissolved CO_2 concentrations, offsetting the decreased physical solubility of the gas in warmer waters (Dam et al., 2021). This interpretation is reinforced by negative correlations with DO during ebb tide (ρ = -0.455; $p < 0.01$), suggesting an association between more oxygenated conditions and lower CO_2 emissions (Xi et al., 2024). However, no significant correlation was detected between aquatic FCO2 and ORP in any tidal phase (flood: ρ = -0.300, $p > 0.05$; ebb: ρ = -0.193, $p > 0.05$). Conversely, the positive correlation with EC during ebb tide (ρ = 0.476; $p < 0.01$), may reflect the influx of interstitial water enriched in ions and carbon, but could also result from water mass mixing during tidal cycles (M. Liu et al., 2025).

The soil, as characterized by Aroni et al. (2026), is acidic (pH 4.2), with a silty texture (74% silt) and low sand content (1.8%). Total organic carbon (1.95%) is considered moderate to high for floodplain soils, indicating organic matter accumulation, possibly associated with the observed acidity (Junk et al., 2011). Nitrogen limitation is evidenced by low total N content (1.7 g kg^{-1}) and a high microbial C/N ratio (43:1), well above the average expected for tropical soils (Duah-Yentumi et al., 1998). These characteristics, coupled with the silty texture, favor water and organic matter retention, creating favorable conditions for microbial activity and the observed CO_2 emissions (Davidson & Janssens, 2006). Nevertheless, the pronounced acidity and very high microbial C/N ratio suggest that decomposer activity may be constrained by nitrogen availability, with microorganisms preferentially cycling carbon rather than mineralizing nitrogen (Z. Chen et al., 2024), or alternatively, enhancing soil N immobilization (José Henrique Cattanio et al., 2008).

The FCH4 were substantially higher in the aquatic environment (0.665 ± 0.137 g CH_4 m^{-2} d^{-1} during ebb tide; 0.173 ± 0.067 g CH_4 m^{-2} d^{-1} during flood tide) than from the soil (0.019 ± 0.003 g CH_4 m^{-2} d^{-1} during ebb tide; 0.015 ± 0.004 g CH_4 m^{-2} d^{-1} during flood tide). On average, water CH_4 fluxes were approximately 27-fold greater than soil fluxes, with a maximum difference of 0.646 ± 0.137 g CH_4 m^{-2} d^{-1} during ebb tide. By comparison, previous records from the same site on high-elevation topography reported soil FCH4 of 0.003 g CH_4 m^{-2} d^{-1}, with topographic variation attributed to water table depth, soil moisture, and organic carbon content (Aroni et al., 2026). Classical studies in the Amazon floodplain reported FCH4 values of 0.027 for open waters, 0.192 for flooded forest, and 0.230 g CH_4 m^{-2} d^{-1} for floating macrophyte banks (Bartlett et al., 1988). The aquatic environment can remain permanently or periodically

https://doi.org/10.5194/egusphere-2026-6918
Preprint. Discussion started: 23 November 2026
© Author(s) 2026. CC BY 4.0 License.

anoxic at the sediment layer, where organic matter is degraded by methanogenic microorganisms (Morin et al., 2018). Methane produced in this manner can reach the atmosphere via ebullition, diffusion through the water column, or transport through roots and tissues of aquatic plants (Bartlett et al., 1988). Ebullition may contribute substantially, accounting for approximately 85% of emissions in floodplain environments (Devol et al., 1988).

In contrast, the water column, particularly during ebb tide, can accumulate CH_4 produced in the sediment and transported by diffusion or advective flows, acting as a reactor from which the gas is released to the atmosphere. Tidal pumping is considered the primary regulator of interstitial water exchange and dissolved CO_2 export in mangrove estuaries, whit a exchange rates ranging between 2.68 and 9.37 g CO_2 m^{-2} d^{-1}, equivalent to approximately 94% of total CO_2 entering the estuary (X. Chen et al., 2021). Our results show that ebb tide in the floodplain forest area increased CO_2 emissions by 2.32-fold in water and 1.35-fold in soil, a pattern consistent with this mechanism.

Collectively, these findings demonstrate that accurately representing greenhouse gas fluxes in tidally influenced floodplains requires integrated soil and water sampling that encompasses both diel and tidal cycles. The relative predominance of CO_2 from soil and CH_4 from water underscores that these two gases respond to distinct production, oxidation, and transport processes. Nevertheless, the absence of direct measurements of aquatic metabolism, dissolved carbon, and ebullition limits the causal attribution of the observed patterns, highlighting the need for future studies that incorporate these variables to more fully constrain the mechanisms driving greenhouse gas dynamics in these complex ecosystems.

4.2 The Role of Ebb Tide in Water Emissions

Our results demonstrated that CO_2 fluxes were higher during ebb tide in both the water column and the soil, albeit with distinct patterns between compartments. In the water column, the mean increase of 4.67 g CO_2 m^{-2} d^{-1} during ebb tide relative to flood tide (Figure 3D) is consistent with the hypothesis that a reduced water depth decreases resistance to gas–atmosphere transfer, thereby facilitating gas escape. Although this mechanism was not directly quantified in the present study, this pattern aligns with observations by Jacotot et al. (2018) in coastal ecosystems, where ebb tide also promoted elevated CO_2 emissions. Similarly, studies in Amazonian mangrove areas

https://doi.org/10.5194/egusphere-2026-6918
Preprint. Discussion started: 23 November 2026
© Author(s) 2026. CC BY 4.0 License.

have reported that ebb tide increased aquatic CO_2 emissions by 1.86-fold and soil emissions by 1.23-fold (Castellón et al., 2021).

In the floodplain forest soil, the effect of tidal phase was more constrained and depended on the interaction between season and tidal type. The overall mean flux was 3.67 g CO_2 m^{-2} d^{-1} higher during ebb tide, but the most pronounced differences occurred under specific conditions, i.e. during the rainy season combined with neap tide, emissions increased by 13.840 g CO_2 m^{-2} d^{-1} (from 2.743 to 16.582 g m^{-2} d^{-1}), and during the dry season combined with spring tide, emissions increased by 4.950 g m^{-2} d^{-1} (from 10.712 to 17.718 g m^{-2} d^{-1}). This pattern suggests that the effect of tidal phase on soil FCO2 is modulated by water column height and antecedent water saturation (Aroni et al., 2026). Similar findings have been reported by Stolpmann et al. (2025) in salt marshes, where CO_2 emissions were higher during neap tides (lower water levels) and during ebb phases, associated with sediment exposure and the activation of aerobic respiration.

In contrast, studies such as that of Jacotot et al. (2018) observed higher CO_2 emissions during spring tides, attributing this effect to greater tidal amplitude and consequent sediment resuspension. Our study, however, showed that spring tide enhanced CO_2 emissions only in the soil during the dry season, suggesting that the effect of tidal amplitude depends on the balance between sediment exposure, which stimulates respiration, and prolonged inundation, which limits oxygen diffusion. Although the main effect of tidal type was not significant in the global model ($p > 0.05$), specific contrasts revealed differences between certain season–tidal type combinations. These contrasts should be interpreted as conditional responses rather than as evidence of a general spring-tide effect. This complexity indicates that tidal type does not operate in isolation but rather in synergy with hydrological seasonality, as previously noted by Guo et al. (2023) for Amazonian floodplain lakes.

4.3 FCH4 Dynamics: Functional Decoupling Between Soil and Water

The most striking finding of this study was that the water compartment becomes a significantly larger source of CH_4 during ebb tide, with a mean difference of 0.646 ± 0.137 g CH_4 m^{-2} d^{-1} relative to the soil. This result reveals a functional decoupling between compartments, while soil CH_4 fluxes remained relatively stable across tidal phases (flood: 0.015 ± 0.004; ebb: 0.019 ± 0.003 g CH_4 m^{-2} d^{-1}; $p > 0.05$), the water column responded intensely to tidal recession, with emissions increasing 3.85-fold

https://doi.org/10.5194/egusphere-2026-6918
Preprint. Discussion started: 23 November 2026
© Author(s) 2026. CC BY 4.0 License.

(95% CI: 1.790–11.150) from 0.173 ± 0.067 g CH_4 m^{-2} d^{-1} during flood to 0.665 ± 0.137 g CH_4 m^{-2} d^{-1} during ebb. During the rainy season combined with spring tides, water fluxes reached even more expressive values, attaining up to 1.620 ± 0.615 g CH_4 m^{-2} d^{-1} under specific conditions (n = 36; maximum = 19.200 g CH_4 m^{-2} d^{-1}).

This pattern is consistent with the mechanism proposed by Su et al. (2024), who demonstrated that sediment exposure during low tide increases CH_4 consumption via methanotrophy by up to 227%, thereby reducing direct soil emissions by approximately 62%. Simultaneously, however, the overlying water, which received CH_4 accumulated during the inundation period, releases this gas more intensely during ebb tide, when the reduced water column thickness lowers diffusion resistance. This effect is amplified by tide-induced pumping, which releases gases trapped in sediment pores and within the water column, a process already described for the Amazon estuary (Ward et al., 2017).

The observed interaction between compartment and tidal phase confirms that the role of water as either a source or a sink of CH_4 is dynamic and tide-dependent. Tidal recession can create steep redox gradients in the surface sediment, driving intensive CH_4 cycling and resulting in elevated emissions to the atmosphere (Tu et al., 2025). This mechanism appears to be particularly active during spring tides, when greater tidal amplitude promotes a more pronounced effect on CH_4 release from the water column, with emission increases of up to 2.56-fold during ebb, a value comparable to that reported for ebb tides in mangrove areas of the Amazon estuary (Castellón et al., 2021).

4.4 The Role of Ebullition and Oxidation in Soil–Water Differences

The lower CH_4 emission from the soil, particularly during ebb tide, can be attributed to greater sediment exposure to the atmosphere, which favors aerobic methane oxidation in the unsaturated zone. This process is consistent with observations by Barbosa et al. (2021), who demonstrated that ebullition varies strongly with water level and its recession rate, with the highest fluxes occurring during falling water periods in flooded forests. Under exposed soil conditions, the contribution of ebullition to total flux may be reduced, whereas the aquatic environment favors both CH_4 production and transport, especially via diffusion and ebullition.

The high proportion of CH_4 consumption in the soil during ebb tide (32.1% of observations) reinforces the role of aerobic exposure in activating methanotrophy. This result aligns with the literature, which indicates that aerobic methane oxidation activity

https://doi.org/10.5194/egusphere-2026-6918
Preprint. Discussion started: 23 November 2026
© Author(s) 2026. CC BY 4.0 License.

is limited by oxygen availability in surface sediments, itself controlled by tidal dynamics (Su et al., 2024). Moreover, it has been observed that surface microbial communities subjected to prolonged air exposure during low tide differ significantly from subsurface communities, a pattern consistent with the hypothesis that aerobic exposure may select for specialized methanotrophic populations (Tu et al., 2025). The lower frequency of CH_4 consumption in the soil during flood tide (11.2%) and the high proportion of neutral fluxes (51.7%) suggest that, under inundated conditions, methanotrophic activity is constrained by low oxygen availability, with anaerobic production likely prevailing. In the water compartment, the transition from a mixed system (34.8% consumption during flood) to a predominantly emitting system (80.6% emission during ebb) indicates that the water column also hosts CH_4 consumption processes, possibly associated with aerobic methanotrophic activity at the water–atmosphere interface.

Comparison with biogeochemical models developed for Amazonian floodplain lakes (Guo et al., 2023) reinforces the importance of hydrodynamic processes in modulating methane emissions, particularly in shallow, warm waters. Our data indicate that, although the soil acts as either a net sink or a moderate source of CH_4 throughout most of the tidal cycle, the water column responds rapidly to hydrological fluctuations, becoming the primary emission pathway during ebb tide.

4.5 Effects of Seasonality and Tidal Type on Fluxes

Our results revealed a complex pattern regarding the influence of seasonality on gas fluxes. When analyzed in isolation, aquatic FCO2 was numerically higher during the rainy season (9.646 ± 1.404 g CO_2 m^{-2} d^{-1}) compared to the dry season (3.308 ± 0.229 g CO_2 m^{-2} d^{-1}). However, the linear mixed-effects model, indicated that season exerted a significant effect on CO_2 emissions in the global model ($F = 7.530$; $p = 0.006$), although the season × compartment interaction ($F = 5.824$; $p = 0.016$) indicates that the seasonal effect differed between water and soil. This outcome shows that while seasonality exhibited important descriptive differences, its effect on CO_2 emissions was modulated by the compartment. For CH_4, no significant seasonal effect was observed in the water compartment ($p = 0.291$). In soil, although the wet/dry ratio was 0.501 (95% CI: 0.272-0.879), the difference was not statistically significant ($p = 0.735$).

The linear mixed models explained 35.7% of the total variation FCH4 (conditional R^2) and 21.8% (marginal R^2). For FCO2, the model with (1|Day/Replicate)

https://doi.org/10.5194/egusphere-2026-6918
Preprint. Discussion started: 23 November 2026
© Author(s) 2026. CC BY 4.0 License.

was singular and conditional R^2 could not be computed; the marginal R^2 of the simplified model (1|Day) was 13.5%. The relatively high contribution of random effects associated with day and hour indicates substantial temporal heterogeneity, suggesting that unmeasured temporal factors play an important role in flux variability. This pronounced temporal variability underscores that high-frequency sampling is essential for accurately quantifying greenhouse gas fluxes in ecosystems subject to tidal regimes.

4.6 Environmental Controls and Explained Variability

Correlation results (Table 3) revealed that tidal height was the most important factor for both gases in the surface water, although this correlation was significant only during ebb tides (FCO2: $\rho = -0.601$, $p < 0.001$; FCH4: $\rho = -0.514$, $p < 0.001$), and not during flood tides (FCO2: $\rho = -0.341$, $p > 0.05$; FCH4: $\rho = -0.129$, $p > 0.05$). In the soil compartment, tidal height was not included in the correlation analysis; the only significant correlation with soil FCO2 was relative humidity (ebb: $\rho = -0.474$, $p < 0.001$; total: $\rho = -0.425$, $p < 0.001$), and no significant correlations were observed between soil FCH4 and any environmental parameter. This finding is consistent with the hypothesis that emissions from the water column are influenced by hydrological dynamics, while soil emissions may be governed primarily by biological processes and edaphic conditions.

The negative correlations of aquatic FCO2 with DO and Tw during ebb tide suggest an association between these variables and emissions to the atmosphere. Similar correlations were observed for aquatic CH_4 with tidal height during ebb tide ($\rho = -0.514$; $p < 0.001$), with EC ($\rho = 0.431$; $p < 0.01$) and TDS ($\rho = 0.434$; $p < 0.001$) also during ebb tide. However, no significant correlation was detected between aquatic CH_4 and ORP during flood tide ($\rho = 0.086$; $p > 0.05$). These patterns are consistent with the literature, where elevated emissions are linked to the formation of steep redox gradients during ebb tide (Tu et al., 2025). It has also been demonstrated that CH_4 oxidation activity is positively correlated with oxygen availability in surface sediments, highlighting the role of oxygen as a key flux controller (Su et al., 2024).

Methane emissions in terrestrial and aquatic ecosystems occur via three main pathways (Couwenberg & Fritz, 2012): (i) molecular diffusion, whereby gas moves through soil pore spaces in response to the concentration gradient between sediment and atmosphere; (ii) ebullition, when CH_4 bubbles formed in waterlogged sediments grow until they exceed the confining pressure of the overlying soil, resulting in abrupt

https://doi.org/10.5194/egusphere-2026-6918
Preprint. Discussion started: 23 November 2026
© Author(s) 2026. CC BY 4.0 License.

releases (Butterbach-Bahl et al., 2011); and (iii) plant-mediated transport, in which CH_4 produced in the sediment is transported through aerenchyma tissues of vascular plants and escapes directly to the atmosphere (Butterbach-Bahl et al., 2011).

In the present study, the elevated CH_4 fluxes observed in the water column, particularly during ebb tide, are consistent with a potentially important contribution from ebullition, as observed in other Amazonian floodplain environments (Barbosa et al., 2021; Ward et al., 2017), where ebullition can account for up to 93% of total CH_4 flux under certain conditions. However, since ebullition was not directly quantified in this study, leaving its relative contribution uncertain, its potential importance is supported by classic findings attributing ~85% of CH_4 emissions in Amazonian floodplains to this pathway (Devol et al., 1988). The pronounced difference between aquatic and soil fluxes underscores the need to separate diffusive and ebullitive transport; automated algorithms (Hoffmann et al., 2017) show that both can equally contribute to total emissions in rewetted wetlands. Our observed elevated water-column fluxes during ebb tide are consistent with significant ebullitive contributions documented in Amazonian systems (Barbosa et al., 2021; Ward et al., 2017).

In contrast, diffusion appears to be the predominant pathway for soil CH_4 emissions, where rates are considerably lower (0.015–0.019 g CH_4 m^{-2} d^{-1}), and sediment exposure during ebb tide favors aerobic methane oxidation by methanotrophs (Su et al., 2024; Tu et al., 2025). Plant-mediated transport, while potentially relevant in areas of dense aquatic vegetation, was not directly quantified in this study, but may have contributed to the emissions observed in the water column during flood tide, when the floodplain forest remains inundated (Barbosa et al., 2021; Bartlett et al., 1988).

The relative contribution of these three pathways to global CH_4 emissions is highly variable across ecosystems, modulated by factors such as sediment porosity, vegetation type, temperature, and hydrological regime (Baur et al., 2024; Sanches et al., 2019). In the context of the present study, our results indicate that ebb tide may act as a trigger for intensified CH_4 release from the water column, whereas in the soil, diffusion and aerobic oxidation appear to predominate. This functional decoupling between compartments, with water acting as the preferential pathway for ebullitive emissions and soil functioning as a predominantly diffusive and oxidative system, reinforces the need for integrated approaches to accurately quantify CH_4 fluxes in tidally influenced floodplain ecosystems.

https://doi.org/10.5194/egusphere-2026-6918
Preprint. Discussion started: 23 November 2026
© Author(s) 2026. CC BY 4.0 License.

5 CONCLUSION

This study provides the first simultaneous quantification of CO_2 and CH_4 fluxes from soil and water in an Amazonian estuarine floodplain forest under direct tidal influence. Our results demonstrate a clear functional decoupling between the compartments, as while the soil acted as the main source of CO_2, the water column was the main emission pathway for CH_4. The tidal phase was a key factor in gas exchange, with ebb tide consistently increasing emissions relative to flood tide. This effect was most pronounced for CH_4 in the water column, where emissions increased 3,850-fold from flood to ebb tide, a much stronger response than previously reported for Amazonian floodplains. CO_2 emissions also increased significantly during ebb tide in both compartments (1,350-fold in soil; 2,320-fold in water), while CH_4 fluxes in soil remained low and stable throughout the tidal phases.

Tidal type had no significant effect on GHG fluxes, and seasonality influenced CO_2 fluxes only through its interaction with compartment, indicating that short-term tidal-phase control over emissions was largely maintained across seasonal and astronomical contexts. Water column emissions were mainly associated with tidal height and physicochemical parameters (EC, TDS, DO, Tw), while soil emissions showed no consistent correlation with environmental variables, possibly reflecting a predominantly biological rather than physical control in the terrestrial compartment. The interaction between compartment and tidal phase was significant for CO_2, but not for CH_4. The magnitude of CH_4 emissions during low tide underscores that coastal freshwater forests can act as disproportionately strong episodic sources of CH_4 to the atmosphere, when diffusion resistance decreases and sediment-derived methane is rapidly released.

These results emphasize that accurate GHG accounts for Amazonian tidal floodplains require integrated soil and water sampling designs that capture both diurnal and tidal cycles, and that short-term or single-compartment measurements likely underestimate emissions. Future studies should quantify the relative contributions of diffusion, ebullition, and plant-mediated transport to constrain the mechanisms driving the pronounced ebb tide CH_4 pulse observed here.

Acknowledgements

https://doi.org/10.5194/egusphere-2026-6918
Preprint. Discussion started: 23 November 2026
© Author(s) 2026. CC BY 4.0 License.

We would like to thank the residents of Ilha do Combú, especially Mr. Odinaldo Pena Quaresma (Didito) and his wife Mrs. Dóris Lucia Santos Mattos da Cunha for their support in the fieldwork. We thank the Coordination for the Improvement of Higher Education Personnel (CAPES) for the financial support during the development of Mario F. Aroni's doctoral thesis.

Code/Data availability

The raw CO_2 and CH_4 flux data, together with the environmental parameters measured during the eight sampling campaigns, are available from the corresponding author upon reasonable request. No custom code was developed for this study; all statistical analyses were performed using the R packages listed in Section 2.6.

Author contribution

José Henrique Cattanio (JHC) and Mario Flores Aroni (MFA) planned the study, which was part of MFA's doctoral thesis. MFA and JHC carried out the field measurements, and JHC conducted the statistical analyses using DeepSeek for script development and R Studio for statistical analyses. JHC supervised the research and prepared this manuscript, with contributions from MFA.

Competing interests

The authors declare that they have no conflict of interest.

References

Abichou, T., Chanton, J., Powelson, D., Fleiger, J., Escoriaza, S., Lei, Y., & Stern, J. (2006). Methane flux and oxidation at two types of intermediate landfill covers. *Waste Management*, *26*(11), 1305–1312. https://doi.org/10.1016/j.wasman.2005.11.016

Abril, G., Martinez, J.-M. M., Artigas, L. F., Moreira-Turcq, P., Benedetti, M. F., Vidal, L., et al. (2014). Amazon River carbon dioxide outgassing fuelled by wetlands. *Nature*, *505*(7483), 395–398. https://doi.org/10.1038/nature12797

Almeida, R. M., Pacheco, F. S., Barros, N., Rosi, E., & Roland, F. (2017). Extreme floods increase CO 2 outgassing from a large Amazonian river. *Limnology and Oceanography*, *62*(3), 989–999. https://doi.org/10.1002/lno.10480

Anderson, A. B. (1990). Alternatives to deforestation: steps towards sustainable use of

https://doi.org/10.5194/egusphere-2026-6918
Preprint. Discussion started: 23 November 2026
© Author(s) 2026. CC BY 4.0 License.

the Amazon rain forest. In A. B. Anderson (Ed.), *Extraction and forest management by rural inhabitants in the Amazon estuary.* (pp. 65–85). New York, NY, USA: Columbia University Press.

Aroni, M. F., Cattanio, J. H., & de Carvalho, C. J. R. (2025). Dynamics of Greenhouse Gas Fluxes in Açaí Cultivation: Comparing Amazonian Upland and Floodplain Soils. *Forests*, *16*(6), 944. https://doi.org/10.3390/f16060944

Aroni, M. F., Cattanio, J. H., Jardim, M. A. G., Vasconcelos, S. S., de Carvalho, C. J. R., de Morais, R. S., & Maia, E. T. (2026). Greenhouse gas fluxes in a managed floodplain forest in the Amazon estuary. *Agricultural and Forest Meteorology*, *378*. https://doi.org/10.1016/j.agrformet.2025.110979

Barbosa, P. M., Melack, J. M., Amaral, J. H. F. F., MacIntyre, S., Kasper, D., Cortés, A., et al. (2020). Dissolved methane concentrations and fluxes to the atmosphere from a tropical floodplain lake. *Biogeochemistry*, *148*(2), 129–151. Retrieved from http://link.springer.com/10.1007/s10533-020-00650-1

Barbosa, P. M., Melack, J. M., Amaral, J. H. F., Linkhorst, A., & Forsberg, B. R. (2021). Large Seasonal and Habitat Differences in Methane Ebullition on the Amazon Floodplain. *Journal of Geophysical Research: Biogeosciences*, *126*(7). https://doi.org/10.1029/2020JG005911

Bartlett, K. B., Crill, P. M., Sebacher, D. I., Harriss, R. C., Wilson, J. O., & Melack, J. M. (1988). Methane flux from the central Amazonian floodplain. *Journal of Geophysical Research: Atmospheres*, *93*(D2), 1571–1582. https://doi.org/10.1029/JD093ID02P01571

Bass, A. M., O' Grady, D., Berkin, C., Leblanc, M., Tweed, S., Nelson, P. N., et al. (2013). High diurnal variation in dissolved inorganic C, δ13C values and surface efflux of CO2 in a seasonal tropical floodplain. *Environmental Chemistry Letters*, *11*(4), 399–405. https://doi.org/10.1007/s10311-013-0421-7

Bates, D., Mächler, M., Bolker, B. M., & Walker, S. C. (2015). Fitting Linear Mixed-Effects Models Using lme4. *Journal of Statistical Software*, *67*(1), 1–48. https://doi.org/10.18637/JSS.V067.I01

Baur, P. A., Henry Pinilla, D., & Glatzel, S. (2024). Is ebullition or diffusion more important as methane emission pathway in a shallow subsaline lake? *Science of*

https://doi.org/10.5194/egusphere-2026-6918
Preprint. Discussion started: 23 November 2026
© Author(s) 2026. CC BY 4.0 License.



The Total Environment, *912*, 169112. https://doi.org/10.1016/J.SCITOTENV.2023.169112

Blagodatsky, S., & Smith, P. (2012). Soil physics meets soil biology: Towards better mechanistic prediction of greenhouse gas emissions from soil. *Soil Biology and Biochemistry*, *47*, 78–92. https://doi.org/10.1016/J.SOILBIO.2011.12.015

Bond-Lamberty, B., Bailey, V. L., Chen, M., Gough, C. M., & Vargas, R. (2018). Globally rising soil heterotrophic respiration over recent decades. *Nature*, *560*(7716), 80–83. https://doi.org/10.1038/s41586-018-0358-x

Bowden, R. D., Newkirk, K. M., & Rullo, G. M. (1998). Carbon dioxide and methane fluxes by a forest soil under laboratory-controlled moisture and temperature conditions. *Soil Biology and Biochemistry*, *30*(12), 1591–1597. https://doi.org/10.1016/S0038-0717(97)00228-9

Butterbach-Bahl, K., Kiese, R., & Liu, C. (2011). Measurements of Biosphere–Atmosphere Exchange of CH4 in Terrestrial Ecosystems. *Methods in Enzymology*, *495*, 271–287. https://doi.org/10.1016/B978-0-12-386905-0.00018-8

Castellón, S. E. M., Cattanio, J. H., Berrêdo, J. F., Rollnic, M., Neu, V., & Ribeiro, M. (2021). Spatial and temporal variability of carbon dioxide and methane fluxes in an Amazonian estuary. *International Journal of Hydrology*, *5*(6), 327–336. https://doi.org/10.15406/ijh.2021.05.00294

Cattanio, José H., Anderson, A. B., & Carvalho, M. S. (2002). Floristic composition and topographic variation in a tidal floodplain forest in the Amazon Estuary. *Revista Brasileira de Botânica*, *25*(4), 419–430. https://doi.org/10.1590/S0100-84042002012000006

Cattanio, José Henrique, Kuehne, R., & Vlek, P. L. G. (2008). Organic material decomposition and nutrient dynamics in a mulch system enriched with leguminous trees in the Amazon. *Revista Brasileira de Ciência Do Solo*, *32*(3), 1073–1086. https://doi.org/10.1590/S0100-06832008000300016

Chen, X., Santos, I. R., Call, M., Reithmaier, G. M. S., Maher, D., Holloway, C., et al. (2021). The mangrove CO2 pump: Tidally driven pore-water exchange. *Limnology and Oceanography*, *66*(4), 1563–1577. https://doi.org/10.1002/lno.11704

Chen, Z., Zhang, H., Tu, X., Wang, J., Elrys, A. S., Tang, Q., et al. (2024). C/N ratio of

https://doi.org/10.5194/egusphere-2026-6918
Preprint. Discussion started: 23 November 2026
© Author(s) 2026. CC BY 4.0 License.

high-organic C materials is a poor predictor of microbial nitrate immobilization potential in a nitrate-rich soil: An 15N incubation study. *Soil and Tillage Research*, *238*, 106019. https://doi.org/10.1016/J.STILL.2024.106019

Conrad, R. (1996). Soil microorganisms as controllers of atmospheric trace gases (H2, CO, CH4, OCS, N2O, and NO). *Microbiological Reviews*, *60*(4), 609–640. https://doi.org/10.1128/mr.60.4.609-640.1996

Conrad, R., Noll, M., Claus, P., Klose, M., Bastos, W. R., & Enrich-Prast, A. (2011). Stable carbon isotope discrimination and microbiology of methane formation in tropical anoxic lake sediments. *Biogeosciences*, *8*(3), 795–814. https://doi.org/10.5194/bg-8-795-2011

Couwenberg, J., & Fritz, C. (2012). Towards Developing IPCC Methane 'Emission Factors' for Peatlands (Organic Soils). *1819-754X*, *10*, 1–17. https://doi.org/10.19189/001C.128455

Dam, B. R. Van, Lopes, C. C., Polsenaere, P., Price, R. M., Rutgersson, A., & Fourqurean, J. W. (2021). Water temperature control on CO2 flux and evaporation over a subtropical seagrass meadow revealed by atmospheric eddy covariance. *Limnology and Oceanography*, *66*(2), 510–527. https://doi.org/10.1002/LNO.11620

Davidson, E. A., & Janssens, I. A. (2006). Temperature sensitivity of soil carbon decomposition and feedbacks to climate change. *Nature*, *440*(7081), 165–173. https://doi.org/10.1038/nature04514

Davidson, E. A., Belk, E., & Boone, R. D. (1998). Soil water content and temperature as independent or confounded factors controlling soil respiration in a temperate mixed hardwood forest. *Global Change Biology*, *4*(2), 217–227. https://doi.org/10.1046/j.1365-2486.1998.00128.x

Davidson, E. A., Verchot, L. V, Cattânio, J. H., Ackerman, I. L., & Carvalho, J. E. M. (2000). Effects of soil water content on soil respiration in forests and cattle pastures of eastern Amazonia. *Biogeochemistry*, *48*(1), 53–69. https://doi.org/10.1023/A:1006204113917

Devol, A. H., Richey, J. E., Clark, W. A., King, S. L., & Martinelli, L. A. (1988). Methane emissions to the troposphere from the Amazon floodplain. *Journal of*

https://doi.org/10.5194/egusphere-2026-6918
Preprint. Discussion started: 23 November 2026
© Author(s) 2026. CC BY 4.0 License.

Geophysical Research, *93*(D2), 1583–1592. https://doi.org/10.1029/JD093iD02p01583

Duah-Yentumi, S., Rønn, R., & Christensen, S. (1998). Nutrients limiting microbial growth in a tropical forest soil of Ghana under different management. *Applied Soil Ecology*, *8*(1–3), 19–24. https://doi.org/10.1016/S0929-1393(97)00070-X

Fox, J., & Weisberg, S. (2019). *An R Companion to Applied Regression* (Third). Thousand Oaks, CA: Sage Publications. Retrieved from https://www.sagepub.com/shop/buy-a-book/an-r-companion-to-applied-regression-3-246125

Gregório, A. M. da S., & Mendes, A. C. (2009a). Batimetria e Sedimentologia da Baía de Guajará, Belém, Estado do Pará, Brasil. *Amazônia: Ci. & Desenv*, *5*(9), 53–72. Retrieved from https://repositorio.museu-goeldi.br/handle/mgoeldi/369

Gregório, A. M. da S., & Mendes, A. C. (2009b). Characterization of sedimentary deposits at the confluence of two tributaries of the Pará River estuary (Guajará Bay, Amazon). *Continental Shelf Research*, *29*(3), 609–618. https://doi.org/10.1016/j.csr.2008.09.007

Guo, M., Melack, J. M., Zhou, W., Barbosa, P. M., Amaral, J. H. F., & Zhuang, Q. (2023). Linking Biogeochemical and Hydrodynamic Processes to Model Methane Fluxes in Shallow, Tropical Floodplain Lakes. *Journal of Advances in Modeling Earth Systems*, *15*(12). https://doi.org/10.1029/2022MS003385

Han, M., & Zhu, B. (2020). Changes in soil greenhouse gas fluxes by land use change from primary forest. *Global Change Biology*, *26*(4), 2656–2667. https://doi.org/10.1111/gcb.14993

Harrell Jr, F. E. (2003, July 17). Hmisc: Harrell Miscellaneous. *CRAN: Contributed Packages*. https://doi.org/10.32614/CRAN.package.Hmisc

Hoffmann, M., Schulz-Hanke, M., Garcia Alba, J., Jurisch, N., Hagemann, U., Sachs, T., et al. (2017). A simple calculation algorithm to separate high-resolution CH 4 flux measurements into ebullition- and diffusion-derived components. *Atmospheric Measurement Techniques*, *10*(1), 109–118. https://doi.org/10.5194/amt-10-109-2017

Huang, J., Luo, M., Liu, Y., Zhang, Y., & Tan, J. (2019). Effects of Tidal Scenarios on

https://doi.org/10.5194/egusphere-2026-6918
Preprint. Discussion started: 23 November 2026
© Author(s) 2026. CC BY 4.0 License.

the Methane Emission Dynamics in the Subtropical Tidal Marshes of the Min River Estuary in Southeast China. *International Journal of Environmental Research and Public Health*, *16*(15), 2790. https://doi.org/10.3390/ijerph16152790

Huttunen, J. T., Väisänen, T. S., Heikkinen, M., Hellsten, S., Nykänen, H., Nenonen, O., & Martikainen, P. J. (2002). Exchange of CO2, CH4 and N2O between the atmosphere and two northern boreal ponds with catchments dominated by peatlands or forests. *Plant and Soil*, *242*, 137–146. https://doi.org/10.1023/A:1019606410655

INMET. (2025). Instituto Nacional de Meteorologia. Retrieved May 14, 2025, from http://www.inmet.gov.br/portal/index.php?r=bdmep/bdmep

IPCC. (2001). *Impacts, Adaptation and Vulnerability, Contribution of Working Group II to the Third Assessment Report of the Intergovernmental Panel on Climate Change*. (J. J. McCarthy, O. F. Canziani, N. A. Leary, D. J. Dokken, & K. S. White, Eds.). Cambridge, UK, and New York, USA.

IPCC. (2014). *Climate Change 2014: Synthesis Report. Contribution of Working Groups I, II and III to the Fifth Assessment Report of the Intergovernmental Panel on Climate Change*. (P. R. K & L. A. Meyer, Eds.). Geneva, Switzerland. https://doi.org/10.1016/S0022-0248(00)00575-3

Jacotot, A., Marchand, C., & Allenbach, M. (2018). Tidal variability of CO2 and CH4 emissions from the water column within a Rhizophora mangrove forest (New Caledonia). *Science of The Total Environment*, *631–632*, 334–340. https://doi.org/10.1016/j.scitotenv.2018.03.006

Junk, W. J., Piedade, M. T. F., Schöngart, J., Cohn-Haft, M., Adeney, J. M., & Wittmann, F. (2011). A classification of major naturally-occurring amazonian lowland wetlands. *Wetlands*, *31*(4), 623–640. https://doi.org/10.1007/S13157-011-0190-7

Kirschke, S., Bousquet, P., Ciais, P., Saunois, M., Canadell, J. G., Dlugokencky, E. J., et al. (2013). Three decades of global methane sources and sinks. *Nature Geoscience*, *6*(September), 813–823. https://doi.org/10.1038/ngeo1955

Kuznetsova, A., Brockhoff, P. B., & Christensen, R. H. B. (2017). lmerTest Package: Tests in Linear Mixed Effects Models. *Journal of Statistical Software*, *82*(13), 1–

https://doi.org/10.5194/egusphere-2026-6918
Preprint. Discussion started: 23 November 2026
© Author(s) 2026. CC BY 4.0 License.

26. https://doi.org/10.18637/JSS.V082.I13

Lenth, R. V., & Piaskowski, J. (2017). emmeans: Estimated Marginal Means, aka Least-Squares Means. *CRAN: Contributed Packages*. https://doi.org/10.32614/CRAN.PACKAGE.EMMEANS

Liu, M., Tian, X., Yan, Z., Zhao, Y., & Li, S. (2025). Diurnal Variation of Carbon Dioxide Concentration and Flux in a River–Lake Continuum of a Mega City. *Water (Switzerland)*, *17*(3), 306. https://doi.org/10.3390/W17030306/S1

Liu, X., Liu, X., Zhu, D., Wang, J., Wang, Z., Liu, W., et al. (2026). Water-level operation creates redox windows that govern greenhouse-gas pathways in reservoir drawdown soils. *Journal of Environmental Management*, *411*, 130130. https://doi.org/10.1016/J.JENVMAN.2026.130130

Mahesh, P., Sreenivas, G., Rao, P. V. N. N., Dadhwal, V. K., Sai Krishna, S. V. S. S., & Mallikarjun, K. (2015). High-precision surface-level CO2 and CH4 using off-axis integrated cavity output spectroscopy (OA-ICOS) over Shadnagar, India. *International Journal of Remote Sensing*, *36*(22), 5754–5765. https://doi.org/10.1080/01431161.2015.1104744

Marinha do Brasil. (2020). Tábuas de Maré - Porto de Belém 2019 - 2020: Centro de Hidrografia da Marinha. Retrieved from https://www.marinha.mil.br/chm/

Morin, T. H., Rey-Sánchez, A. C., Vogel, C. S., Matheny, A. M., Kenny, W. T., & Bohrer, G. (2018). Carbon dioxide emissions from an oligotrophic temperate lake: An eddy covariance approach. *Ecological Engineering*, *114*, 25–33. https://doi.org/10.1016/j.ecoleng.2017.05.005

Nakano, T., Sawamoto, T., Morishita, T., Inoue, G., & Hatano, R. (2004). A comparison of regression methods for estimating soil-atmosphere diffusion gas fluxes by a closed-chamber technique. *Soil Biology and Biochemistry*, *36*(1), 107–113. https://doi.org/10.1016/j.soilbio.2003.07.005

Nittrouer, C. A., & Kuehl, S. A. (1995). Geological significance of sediment transport and accumulation on the Amazon continental shelf. *Marine Geology*, *125*(3–4), 175–176. https://doi.org/10.1016/0025-3227(95)00073-8

Norman, J. M., Kucharik, C. J., Gower, S. T., Baldocchi, D. D., Crill, P. M., Rayment, M., et al. (1997). A comparison of six methods for measuring soil-surface carbon

https://doi.org/10.5194/egusphere-2026-6918
Preprint. Discussion started: 23 November 2026
© Author(s) 2026. CC BY 4.0 License.

dioxide fluxes. *Journal of Geophysical Research: Atmospheres*, *102*(D24), 28771–28777. https://doi.org/10.1029/97JD01440

Peel, M. C., Finlayson, B. L., & McMahon, T. A. (2007). Updated world map of the Köppen-Geiger climate classification. *Hydrology and Earth System Sciences*, *11*(5), 1633–1644. https://doi.org/10.5194/hess-11-1633-2007

Pires, J. M., & Prance, G. T. (1985). The vegetation types of the Brazilian Amazon. In G. Prance & T. Lovejoy (Eds.), *Amazonia: Key Environments* (1st Editio, pp. 109–145). Pergamon Press, United Kingdom.

Potter, C., Melack, J. M., & Engle, D. (2014). Modeling methane emissions from amazon floodplain ecosystems. *Wetlands*, *34*(3), 501–511. https://doi.org/10.1007/s13157-014-0516-3

Sanches, L. F., Guenet, B., Marinho, C. C., Barros, N., & de Assis Esteves, F. (2019). Global regulation of methane emission from natural lakes. *Scientific Reports 2019 9:1*, *9*(1), 255-. https://doi.org/10.1038/s41598-018-36519-5

Sawakuchi, H. O., Neu, V., Ward, N. D., Barros, M. de L. C., Valerio, A. M., Gagne-Maynard, W., et al. (2017). Carbon dioxide emissions along the lower Amazon River. *Frontiers in Marine Science*, *4*(MAR), 1–12. https://doi.org/10.3389/fmars.2017.00076

Silva, C. A. R., & Sampaio, L. S. (1998). Speciation of phosphorus in a tidal floodplain forest in the Amazon estuary. *Mangroves and Salt Marshes*, *2*(1), 51–57. https://doi.org/10.1023/A:1009950208582

Stanley, E. H., Casson, N. J., Christel, S. T., Crawford, J. T., Loken, L. C., & Oliver, S. K. (2016). The ecology of methane in streams and rivers: patterns, controls, and global significance. *Ecological Monographs*, *86*(2), 146–171. https://doi.org/10.1890/15-1027

Stolpmann, L. M., Balke, T., & Bass, A. M. (2025). Sediment to atmosphere CO2 efflux increases at retreating salt marsh edges. *Estuarine, Coastal and Shelf Science*, *313*, 109129. https://doi.org/10.1016/J.ECSS.2025.109129

Su, G., Guo, Z., Hu, Y., Zheng, Q., Zopfi, J., Lehmann, M. F., & Jiao, N. (2024). Tidal control on aerobic methane oxidation and mitigation of methane emissions from coastal mangrove sediments. *Environmental Research*, *263*(P1), 120049.

https://doi.org/10.5194/egusphere-2026-6918
Preprint. Discussion started: 23 November 2026
© Author(s) 2026. CC BY 4.0 License.

https://doi.org/10.1016/j.envres.2024.120049

Team, R. C. (2018). A Language and Environment for Statistical Computing. *R Foundation for Statistical Computing*. https://doi.org/10.4236/oalib.1107821

Tu, T. H., Lee, T. Y., Yu, Z. H., Lu, C. H., Lin, Y. T., & Wang, P. L. (2025). Methane dynamics controlled by subsurface metabolic architecture and tidal cycling in a mangrove wetland. *Science of the Total Environment*, *988*(1), 179769. https://doi.org/10.1016/j.scitotenv.2025.179769

Wang, Z. Y., Xie, J. B., Wang, Y. G., & Li, Y. (2020). Biotic and Abiotic Contribution to Diurnal Soil CO2 Fluxes from Saline/Alkaline Soils. *Scientific Reports*, *10*(1), 5396. https://doi.org/10.1038/s41598-020-62209-2

Ward, N. D., Bianchi, T. S., Medeiros, P. M., Seidel, M., Richey, J. E., Keil, R. G., & Sawakuchi, H. O. (2017). Where Carbon Goes When Water Flows: Carbon Cycling across the Aquatic Continuum. *Frontiers in Marine Science*, *4*. https://doi.org/10.3389/fmars.2017.00007

Wei, S., Han, G., Chu, X., Song, W., He, W., Xia, J., & Wu, H. (2020). Effect of tidal flooding on ecosystem CO2 and CH4 fluxes in a salt marsh in the Yellow River Delta. *Estuarine, Coastal and Shelf Science*, *232*(December 2019), 106512. https://doi.org/10.1016/j.ecss.2019.106512

Wickham, H. (2016). *ggplot2: Elegant Graphics for Data Analysis*. Springer-Verlag New York. Retrieved from https://ggplot2.tidyverse.org

Wickham, H., & Bryan, J. (2015, April 14). readxl: Read Excel Files. *CRAN: Contributed Packages*. https://doi.org/10.32614/CRAN.package.readxl

Wickham, H., Vaughan, D., & Girlich, M. (2014, July 21). tidyr: Tidy Messy Data. *CRAN: Contributed Packages*. https://doi.org/10.32614/CRAN.package.tidyr

Wickham, H., François, R., Henry, L., Müller, K., & Vaughan, D. (2026). dplyr: A Grammar of Data Manipulation. https://doi.org/10.32614/CRAN.package.dplyr

WMO. (2015). WMO Greenhouse Gas Bulletin - The State of Greenhouse Gases in the Atmosphere Based on Global Observations through 2014. *World Meteorological Organization and Global Atmosphere Watch, No. 11*(11), 1–4. Retrieved from http://www.theguardian.com/environment/2015/nov/09/earths-climate-entering-new-permanent-reality-as-co2-hits-new-

https://doi.org/10.5194/egusphere-2026-6918
Preprint. Discussion started: 23 November 2026
© Author(s) 2026. CC BY 4.0 License.



high%255Cnpapers3://publication/uuid/1069A331-1272-4EA9-BB0E-DD939C008DC8

Xi, N., Zhang, T., Zhao, W., Jia, Y., Fan, J., Li, R., et al. (2024). Metabolic processes drive spatio-temporal variations of carbon sink/source in a karst river. *Environmental Research*, *262*, 119970. https://doi.org/10.1016/J.ENVRES.2024.119970